Hybrid tri-level optimal sizing of hydrogen storage for addressing long-term seasonal fluctuation of RES

Qianwen Hu, Gengfeng Li, Bingkai Huang, Qiming Yang, Siyuan Sun,
Zhaohong Bie, Jianzhong Wu, Yue Zhou, Yiheng Bian

***Abstract*—Time-varying renewable energy sources (RES), influenced by climate conditions, create seasonal power mismatches. Allocation of hydrogen energy storage (HES) can mitigate long-duration seasonal power mismatch caused by load variation, climate variability and seasonal meteorological conditions. However, one single uncertainty set cannot well consider the characteristics of RES uncertainty in different seasons impacted by long-term climate conditions. To address the above challenges and optimally size and allocate HES in power systems, this paper proposes a hybrid tri-level planning framework that integrates RES interannual long-term and seasonal fluctuation, using a combination of distributionally robust optimization (DRO) and adaptive robust optimization (ARO). Specifically, a RES probability distribution ambiguity set under typical climate conditions is constructed using norm constraints, and data-driven DRO is introduced to address RES long-term uncertainty. RES seasonal uncertainty is then adaptively modelled using multiple uncertainty sets based on the seasonal meteorological characteristics of RES, and ARO is proposed to reformulate the lower-level problem for the worst-case scenarios. The proposed framework is solved using the improved column and constraint generation algorithm (C&CG) with duality-free decomposition. Simulations on IEEE 39-bus system and IEEE 118-bus system confirm the effectiveness of the proposed planning framework and solution algorithm.**

***Index Terms*—hydrogen energy storage (HES); power systems; long-term seasonal uncertainty; optimization planning; robust optimization; climate adaptability.**

NOMENCLATURE

Abbreviations

HES	Hydrogen energy storage.
HT	Hydrogen tank.
P2H	Electrolyzer for hydrogen generation.
FC	Fuel cell for power generation.
LU	Long-term uncertainty of RES.
SU	Seasonal uncertainty of RES.

Sets and Indices

$(i,j)\in\mathcal{L}$	Set of line indices (i,j).
$i\in\mathcal{I}$	Set of node indices i.
$\mathcal{N}^{\mathcal{HS}}/\mathcal{N}^{\mathcal{RS}}/\mathcal{N}^{\mathcal{TG}}$	Set of nodes with HES/RES/TG.
$t\in\mathcal{T}$	Set of time indices t.
$d\in\mathcal{D}$	Set of natural day indices d.
$s\in\mathcal{S}$	Set of typical day scenario indices s.
$n\in\mathcal{N}$	Set of representative long-term RES scenario n.

Parameters

C_{E}	Unit investment cost of HT (\$/kg H_2).
$C_{\mathrm{P}}^{\mathrm{P2H}}$ / $C_{\mathrm{P}}^{\mathrm{FC}}$	Unit investment cost of P2H/FC (\$/MW).
c_w / c_i	Penalty (\$/MWh) of RES/Load curtailment.
c_g / c_g^{su} / c_g^{sd}	Generation cost (\$/MWh)/start-up (\$)/shut-down cost (\$) of TG unit g.
P_w^{W} / P_i^{Load}	Output power (MW) of RES unit w /Load demand (MW) of node i.
x_l / $P_l^{\max}$	Reactance/maximum capacity (MW) of line l.
$\theta_i^{\max}$ / $\theta_i^{\min}$	Maximum/minimum phase angle of node i.
$P_g^{\max}$ / $P_g^{\min}$	Maximum/minimum output power (MW) of TG unit g.
R_g^U / R_g^D	Upward/downward ramping limit (MW) of TG unit g.
R_g^{SU} / R_g^{SD}	Maximum output power (MW) of TG unit g at start-up/shut-down state.
p_n^0	Original probability of representative RES scenario n.

Variables

$\tilde{p}_n$	Probability of representative RES scenario n.
$\tilde{\Delta}_{i,t,s,n}$	Uncertainty power of node i at time t under typical day s of representative RES scenario n.
S_i	HES planning capacity (MW) at node i.
$P_{w,t,s,n}^{\mathrm{W}'}$	Power curtailment (MW) of RES unit w at time t under typical day s of representative RES scenario n.
$P_{i,t,s,n}^{\mathrm{Load}'}$	Load curtailment (MW) of node i.
$P_{g,t,s,n}^{\mathrm{G}}$	Output power (MW) of TG unit g.
$P_{g,t,s,n}^{\mathrm{G,r}}$	Adjustable variable representing reserve capacity (MW) of TG unit g.
$P_{i,t,s,n}^{\mathrm{P2H,Cha}}$	Charge power (MW) of HES unit i at time t under typical day s.

This work was supported by the National Natural Science Foundation of China (U22B20103) and China Scholarship Council. J. Wu's contribution is supported by the EPSRC Hi-ACT Hub (EP/X038823/2) and the UKRI UKERC 2024-2029 project. *(Corresponding author: Gengfeng Li).*

The authors Q. Hu, G. Li, B. Huang, S. Sun, Z. Bie and Y. Bian are with Xi'an Jiaotong University, Xi'an, China (e-mail: qwhu089@stu.xjtu.edu.cn, gengfengli@mail.xjtu.edu.cn, bingkaihuang@stu.xjtu.edu.cn, divinegate@stu.xjtu.edu.cn, zhbie@mail.xjtu.edu.cn, byh0xyz@xjtu.edu.cn). J. Wu and Y. Zhou are with Cardiff University, Cardiff, the United Kingdom (e-mail: WuJ5@cardiff.ac.uk, ZhouY68@cardiff.ac.uk). Q. Yang is with State Grid Shanghai Pudong Power Supply Company, Shanghai, China (e-mail: yangqiming13@gmail.com)

$P_{i,t,s,n}^{\mathrm{FC,Dis}}$	Discharge power (MW) of HES unit i at time t under typical day s.
$P_{i,t,s,n}^{\mathrm{FC,r}}$	Adjustable variable representing reserve capacity (MW) of FC unit i.
$\lambda_{i,t,s,n}^{\mathrm{FC}}$ / $\lambda_{i,t,s,n}^{\mathrm{G}}$	Non-negative continuous variables to indicate participation factor of node i.
$SOC_{i,t,d,n}$	Hydrogen (kg H_2) stored in the tank of HES i at time t under natural day d.
$SOC_{i,t,d,n}^{\mathrm{inter}}$	Inter-day component of SOC.
$SOC_{i,t,s,n}^{\mathrm{intra}}$	Intra-day component of SOC
$P_{l,t,s,n}$	Power flow (MW) of line l.
$\theta_{i,t,s,n}$	Phase angle of node i.
x_i	Binary variable indicating whether HES is allocated at node i (1) or not (0).
$I_{g,t,s,n}$	Binary variable indicating online state (1) or offline state (0) of TG unit g.
$U_{g,t,s,n}$ / $D_{g,t,s,n}$	Binary variable indicating start-up state or shut-down state of TG unit g.

I. INTRODUCTION

Climatic conditions greatly affect the power generation of renewable energy sources (RES) across all timescales, with long-term and seasonal effect included. Long-term climate uncertainty causes interannual variability of photovoltaic power generation (PV) ranges from 6% to 17%, and that of wind power generation ranges between 3% and 9% [1]. Besides the impact of long-term climate uncertainty, RES also follow the seasonal meteorological characteristics, wind speed exhibits greater fluctuation in winter, while solar irradiance varies most in summer [2]. With the increase of RES in power systems to promote low-carbon goals, these climate-driven and time-varying energies raise a huge concern on long-duration seasonal "energy droughts". RES seasonal fluctuation results in power shortage risk during summer and winter, while a large share of RES curtailment occurs in spring and autumn, nearly 70% in China [3]. In addition, long-duration extreme power shortage events, such as extreme high temperature in Sichuan of China 2022 and the dark doldrum event of three days in Germany 2023, also show an uptrend under long-term climate change [4]. Addressing the fluctuation of climate-driven RES means that flexibility resources will be needed to varying extents throughout the year, even on a week-to-week or month-to-month basis. For power system designing with high proportion RES, long-duration seasonal storage of excess RES to realize seasonal regulation will be essential to enhance climate adaptability [5].

It is estimated that 8 TW long duration energy storage is needed for global power systems by 2040 with a market potential of $4 trillion [6]. Hydrogen energy storage (HES), as a long duration energy storage, has outstanding advantages in energy and time dimensions [7]. The storage scale is large (1 million kilowatts level) and the duration time is long (cross-season). Excess RES can be used for hydrogen production and storage. While power supply is insufficient, hydrogen can be converted into electricity by fuel cells, hydrogen fired power plants or other means. HES will play an important role and show an exponential growth in renewable-dominated power systems to address RES seasonal fluctuations [8]. Therefore, reasonable planning of HES in power systems, considering the compounding effects of climate variability and seasonal meteorological conditions on RES uncertainty over time, is of great significance to mitigate long-duration seasonal supply-demand mismatch risks.

Currently, many studies focus on HES planning methods to address seasonal power mismatch in power systems. Different from short-duration energy storage planning, which is based on typical days with only daily cycle of state of charge (SOC) modelled, HES has long-duration cross-season regulation role, so that a whole yearly SOC cycle needs to be considered. For HES optimization planning in power systems, the difficulty is: 1) the HES operation requires considering energy coupling relationship between different days and long-duration storage cycle of a whole year, posing a challenge to the modelling and solving of the optimization problem. 2) HES needs to realize cross-season regulation, characterizing long-term seasonal fluctuation of RES, which is also challenging.

Some studies [9]-[13] describe RES seasonal fluctuation by typical days, and the HES model based on typical days is formulated, with the SOC operation relationship between different typical days considered. Specifically, ref. [9] proposes a HES model based on two typical days (RES abundant and poor day), and a stochastic optimization (SO) method is used to address RES uncertainty. Ref. [10] proposes a scenario generation and cluster method based on eigenvalues to select typical days for considering uncertainty. Ref. [11] proposes a cross-regional HES planning model considering uncertainty by a distributionally robust optimization (DRO) method. Moreover, a two-layer HES model is proposed to describe long-duration operation relationship in [12], [13]. The inter-day layer describes SOC relationship between different typical days. To address the uncertainty of RES, robust optimization (RO) and SO are proposed in [12], [13].

The HES models in above studies describe the SOC coupling relationship between different typical days, which ensure SOC continuity among the selected typical days. However, it is difficult for HES models based on typical days to simulate long-duration dynamics of hydrogen storage in a whole yearly cycle, and it is difficult for using typical days to describe the interannual long-term uncertainty. Therefore, ref. [14] proposes a HES model based on an 8760-hour time series in power systems planning. The inventory change of HES between different days and months in a year is modeled. Nevertheless, considering the operation of 8760 hours causes the model to be too large and time-consuming in solution. To reduce the computational burden, ref. [15] proposes a convex relaxation-based planning model using 8760-hour yearly data for hydrogen-based microgrids. Ref. [16] proposes a HES model using the uniform hierarchical time discretization method. Ref. [17] proposes a least-square-based scenario approximation method to reformulate scenarios based on multiple timescales' fluctuation characteristics decomposed from the 8760h data, and a HES planning model in microgrids

is formulated based on the approximation scenarios. Ref. [3] and [18] propose to decouple the 8760-hour SOC into inter-day and intra-day components for HES optimization planning to reduce the computational burden. In [14]-[18], the whole yearly continuity of SOC is ensured. In addition, ref. [3] and [16] further consider the long-term uncertainty of RES by the SO method.

In summary, most of the existing studies focus on the difficulty in HES modelling caused by multi-timescale planning in microgrids or power distribution systems level. For RES uncertainty, the existing methods use RO [12], SO [3] [9] [13] [16] or DRO [11] methods, by formulating a single uncertainty set to describe RES uncertainty. However, RES uncertainty usually exhibits different characteristics in different seasons due to seasonal meteorological conditions, a single uncertainty set cannot precisely characterize the seasonal fluctuation degrees of RES [19]. Therefore, seasonal uncertainty needs to be further modelled, seasonal uncertainty in this paper refers to the difference in the fluctuation degrees of RES in different seasons of a year due to seasonal meteorological conditions. Besides seasonal uncertainty, RES supply is also strongly impacted by long-term climate conditions, the research of CMIP6 show that long-term climate uncertainty causes huge interannual variability of RES [20]. Long-term climate uncertainty in this paper refers to the interannual variability of RES output power from year to year due to climate variability. Ref. [21]-[22] analyze power mismatch risks under climate change and underline the importance of considering long-term climate variability in power systems planning. Ref. [23]-[24] model long-term extreme events and long-term temperature uncertainty influenced by climate variability in transmission defense planning and zero energy buildings planning. For HES, it can achieve seasonal storage, providing a flexible and resilient solution to address long-term seasonal fluctuations of RES, thus enhance the climate adaptability of power systems. Therefore, in HES planning, long-term seasonal uncertainty of RES impacted by the compounding effects of long-term climate variability and seasonal meteorological conditions over time must be further considered.

Motivated by the above challenges and considering the correlations between long-term and seasonal uncertainty of RES, the main idea of this paper is to combine long-term seasonal uncertainty in HES planning by a hybrid DRO-ARO (adaptive robust optimization) method. DRO is used to deal with long-term uncertainty of RES and find the worst distribution of long-term uncertainty. Then, RES seasonal uncertainty is adaptively modelled as multiple uncertainty sets according to seasonal characteristics. ARO is used to transform seasonal uncertainty problem as a deterministic model for the worst-case reformulation to deal with seasonal uncertainty. Because long-term climate variability is difficult to characterize, the proposed hybrid DRO-ARO method makes robust planning decisions for HES under the worst-case scenarios of long-term seasonal uncertainties, enhancing the adaptability to long-term climate variability and seasonal meteorology. The main contributions of this paper are as below:

1) To address long-term seasonal uncertainty of RES, a tri-level optimization planning framework for HES in power systems is proposed, where a hybrid DRO-ARO method is introduced to manage long-term seasonal fluctuation of RES caused by climate variability and seasonal meteorological conditions.
2) A novel uncertainty set is established based on the multi-year datasets to capture and model long-term seasonal uncertainty of RES. Firstly, the ambiguity set for long-term RES uncertainty is constructed from interannual historical datasets using norm constraints. Then, based on the realization of long-term uncertainty, seasonal uncertainty sets are adaptively modelled according to the seasonal characteristics of RES prediction error distributions.
3) Considering the integration of long-term seasonal uncertainty increases the complexity in model-solving. An improved C&CG algorithm, by leveraging adaptive robust reformulation alongside parallel computation of duality-free decomposition, is applied to solve the proposed tri-level planning model, which mitigates the computational burden and enables an efficient solution process.

The remainder of this paper is organized as follows. Section II illustrates the conceptual planning framework and long-term seasonal uncertainty modelling methods. Section III provides the mathematical formulation of the hybrid tri-level DRO-ARO planning model. Section IV introduces the solution algorithm. Section V presents numerical experiments on the test systems. Finally, Section VI concludes the full paper.

II. Conceptual Framework

In this section, the conceptual framework of the proposed hybrid tri-level DRO-ARO planning model is introduced. Then, RES long-term seasonal uncertainty sets are modelled.

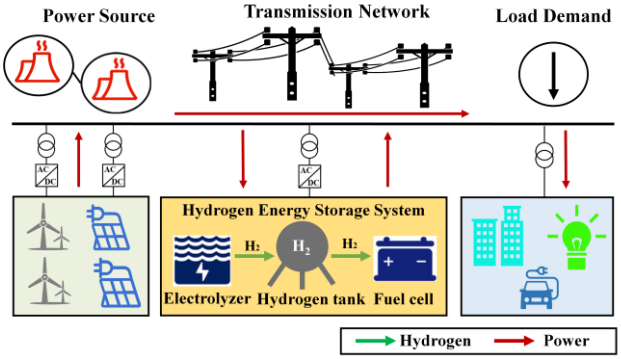

Fig. 1. The structure of power systems with HES.

The main problem we focus on in this paper is how to reasonably allocate HES in powers systems to address long-term seasonal fluctuations of RES. The structure of power systems where HESs are applied is shown in Fig. 1. In power sources of power systems with high proportion of RES, RES influenced by climate conditions are gradually replacing traditional synchronous generators, which will lead to seasonal mismatch between supply and demand. The allocation of HES can realize seasonal regulation by balancing RES output with load demand. The structure of HES which consists of

electrolyzers (P2H) for power-to-hydrogen production, hydrogen tanks (HT) for hydrogen storage and fuel cells (FC) for power generation using hydrogen. During off-peak periods with excess RES output, surplus energy is utilized for hydrogen production and storage. Then, the stored hydrogen is converted into electricity to achieve cross-season regulation when RES supply is insufficient during peak demand periods.

A. Hybrid Tri-level HES Planning Framework

Firstly, the seasonal-trend decomposition using loess (STL) algorithm is used to capture seasonal fluctuation characteristics of RES according to [17]. STL is a common algorithm for decomposing a time series into trend, seasonal and irregular components [25], as given by:

$$T_{\mathrm{W}} = T_{\mathrm{W}}^{\mathrm{Trend}} + T_{\mathrm{W}}^{\mathrm{Seasonal}} + T_{\mathrm{W}}^{\mathrm{Irregular}} \quad (1)$$

For time series such as RES output power T_{W} with random noise, trend and seasonal component describing seasonal trend can be extracted. In this way, the seasonal fluctuations can be preserved for reliable HES planning.

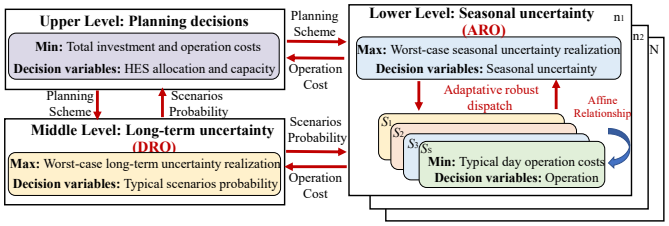

Fig. 2. Tri-level HES planning framework.

Based on the trend and seasonal component of RES, the framework of tri-level planning model for HES is shown in Fig. 2. ARO is to address seasonal uncertainty and reformulate the lower-level seasonal uncertainty problem as a deterministic model for the worst case. The data-driven DRO method is used to address long-term uncertainty in the middle level and the ambiguity set of RES long-term uncertainty is constructed using norm constraints. Specifically, the three levels as shown in Fig. 2 are described as below:

1) Upper Level: the upper level makes "here and now" planning decisions for HES allocation and capacity with the objective function to minimize HES annual investment.

2) Middle Level: the middle level constructs the ambiguity sets of RES long-term uncertainty and try to find the worst distribution using DRO method, with the aim to ensure HES planning results adapt to long-term climate variability.

3) Lower Level: the lower level makes "wait and see" robust operation decisions using ARO method, with the objective function of minimizing power system annual operation costs under the worst case of RES seasonal uncertainty to ensure HES planning results adapt to the impact of seasonal meteorological conditions.

The upper-level HES planning decisions are made based on the operation simulation of the middle and the lower level. The middle level accepts interannual historical information of RES and deals with RES long-term uncertainty using DRO method. In the lower level, based on the worst realization of long-term uncertainty determined in the middle level, seasonal uncertainty sets are then overlaid to make robust operation decisions using ARO method. Then, the operation strategy of the lower-level feed back to the upper-level and the middle level for iteratively solution.

B. RES Long-term Uncertainty Set Modelling

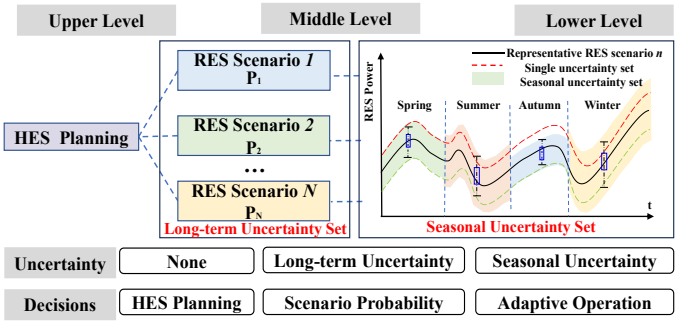

Fig. 3. Illustration of long-term seasonal uncertainty set.

As shown in Fig. 3, RES long-term uncertainty set is modelled and considered in the middle level. RES long-term uncertainty refers to RES variations occurring over multiple years caused by climate variations. To make HES planning results adapt to climate variability, RES interannual long-term historic datasets N^0 are used and reduced to representative scenarios N by scenarios reduction technology to represent RES scenarios of yearly output power under typical climate conditions. A realization of representative RES scenario n is utilized to simulate the impact of RES long-term uncertainty (LU) induced by climate variations. Specifically, in this paper, 5 representative scenarios of 8760-hour RES series obtained from interannual long-term historic datasets are used to model RES long-term uncertainty. The scenario reduction techniques used in our research are k-means clustering algorithm and simultaneous backward reduction (SBR) algorithm in our previous work [26]. And the elbow method is used to determine the optimal number of representative scenarios N, while statistical validation further ensures the representativeness of the selected scenarios, thereby guaranteeing the effectiveness of uncertainty modeling. Then, considering the uncertainty and variability of long-term climate conditions, the first max in the middle level is treated as an uncertain variable of the probability distribution of representative RES scenarios to address RES long-term uncertainty caused by climate variability using a data-driven DRO method. The ambiguity set $\mathcal{P}$ of the probability distribution of RES representative scenarios is constructed by ℓ_1 norm and ℓ_∞ norm constraints in the middle level. Norm constraints allow uncertain probability distribution to fluctuate within a pre-defined confidence set. That is, at a given confidence level, the obtained HES planning results can guarantee to cover all possible probability distributions.

$$\mathcal{P} = \left\{ \tilde{p} \in [0,1] \middle| \sum_{n \in \mathcal{N}} \tilde{p}_n = 1 \right\} \quad (2)$$

$$\mathcal{P} = \left\{ \tilde{p} \in [0,1] \middle| \sum_{n \in \mathcal{N}} \left| \tilde{p}_n - p_n^0 \right| \le \beta_1 \right\} \quad (3)$$

$$\mathcal{P} = \quad \tilde{p} \in [0,1] \middle| \max \left| \tilde{p}_n - p_n^0 \right| \le \beta_\infty, \forall n \in \mathcal{N} \quad (4)$$

$$\beta_1 = \frac{N}{2N^0} \ln \frac{2N}{1-\gamma_1} \tag{5}$$

$$\beta_\infty = \frac{N}{2N^0} \ln \frac{2N}{1-\gamma_\infty} \tag{6}$$

Constraint (2) states the sum of the probability of RES scenarios is equal to 1. ℓ_1 norm constraint (3) and ℓ_∞ norm constraint (4) limits the total and maximum fluctuation degree of the probability distribution of representative RES scenarios, respectively. By parameter β_1 and β_∞ , the uncertainty degree can be further optimized, specifically, as the parameters β_1 and β_∞ increase, the uncertainty become higher, thereby enhancing the robustness of the planning results. The value of β_1 and β_∞ is obtained in (5)-(6) according to [27], where γ_1 and γ_∞ are pre-given confidence level parameters.

C. RES Seasonal Uncertainty Set Modelling

RES seasonal uncertainty set is modelled and considered in the lower level based on a realization of RES long-term uncertainty. RES seasonal uncertainty refers to RES variations occurring within a single year, associated with natural seasonal cycles (winter, spring, summer, fall). In this paper, the average prediction error distribution of RES in different seasons is used to model RES seasonal uncertainty. Specifically, RES seasonal uncertainty is modeled adaptively as multiple uncertainty sets according to RES seasonal characteristics, and then are overlaid on the representative RES scenarios of long-term uncertainty. Compared with using a single uncertainty set (the area between red and green dashed lines in Fig. 3) to describe the possible fluctuation degrees of RES in different seasons, the seasonal uncertainty set in this paper can avoid conservative planning results in some seasons or inadequate adaptation of planning results to RES uncertainty in other seasons. For seasonal uncertainty set modelling, each representative RES scenario has 8760-hour data of output power and the typical day scenarios S_1, S_2, S_3…, S_{S0} can be obtained using the scenarios reduction technology [26]. For different typical days S_1, S_2, S_3…, S_{S0}, RES seasonal uncertainty set is modelled according to the seasonal characteristics of RES prediction error distribution. According to the affine relationship, the original S_0 typical day scenarios under a typical RES long-term uncertainty scenario LU_n become S=4S_0 (SU_1, SU_2, SU_3…, SU_S) after considering RES seasonal uncertainty. The proposed seasonal uncertainty set $\mathcal{U}$ is shown in (7)-(8), where σ_j represents the average prediction error in different season *j* according to [28]. Hence, the uncertainty set {LU_1-SU_1, LU_1-SU_2, LU_1-SU_3…, LU_1-SU_S} can represent a realization of RES seasonal uncertainty under a typical climate condition. Different realization of LU_n-SU_s simulates RES long-term seasonal uncertainty impacted by climate variability and seasonal meteorological conditions.

$$\mathcal{U} = \left\{ \tilde{P}^{\mathrm{W}}_{w,t,s} \middle| \begin{matrix} P^{\mathrm{W}}_{w,t,s_0} - \sigma^w_j P^{\mathrm{W}}_{w,t,s_0} \le \tilde{P}^{\mathrm{W}}_{w,t,s} \le P^{\mathrm{W}}_{w,t,s_0} + \sigma^w_j P^{\mathrm{W}}_{w,t,s_0}, \\ \forall w \in \mathcal{N}^{\mathcal{RS}}, \forall t \in \mathcal{T}, \forall s \in \mathcal{S} \end{matrix} \right\} \tag{7}$$

$$\mathcal{U} = \left\{ \tilde{P}^{\mathrm{Load}}_{i,t,s} \middle| \begin{matrix} P^{\mathrm{Load}}_{i,t,s_0} - \sigma^{\mathrm{L}}_j P^{\mathrm{Load}}_{i,t,s_0} \le \tilde{P}^{\mathrm{Load}}_{i,t,s} \le P^{\mathrm{Load}}_{i,t,s_0} + \sigma^{\mathrm{L}}_j P^{\mathrm{Load}}_{i,t,s_0}, \\ \forall i \in \mathcal{I}, \forall t \in \mathcal{T}, \forall s \in \mathcal{S} \end{matrix} \right\} \tag{8}$$

$$\mathcal{U} = \left\{ \tilde{\Delta}_{i,t,s} \middle| \begin{matrix} \tilde{\Delta}_{i,t,s} = \Delta \tilde{P}^{\mathrm{W}}_{w,t,s} + \Delta \tilde{P}^{\mathrm{Load}}_{i,t,s}, \\ \forall i \in \mathcal{I}, \forall t \in \mathcal{T}, \forall s \in \mathcal{S} \end{matrix} \right\} \tag{9}$$

$$\mathcal{U} = \left\{ \tilde{\Delta}^{\max}_{i,t,s} \middle| \begin{matrix} \tilde{\Delta}^{\max}_{i,t,s} = \sigma^w_j P^{\mathrm{W}}_{w,t,s_0} + \sigma^{\mathrm{L}}_j P^{\mathrm{Load}}_{i,t,s_0}, \\ \forall w \in \mathcal{N}^{\mathcal{RS}}, \forall i \in \mathcal{I}, \forall t \in \mathcal{T}, \forall s \in \mathcal{S} \end{matrix} \right\} \tag{10}$$

$$\mathcal{U} = \left\{ \tilde{\Delta}^{\min}_{i,t,s} \middle| \begin{matrix} \tilde{\Delta}^{\min}_{i,t,s} = -\sigma^w_j P^{\mathrm{W}}_{w,t,s_0} - \sigma^{\mathrm{L}}_j P^{\mathrm{Load}}_{i,t,s_0}, \\ \forall w \in \mathcal{N}^{\mathcal{RS}}, \forall i \in \mathcal{I}, \forall t \in \mathcal{T}, \forall s \in \mathcal{S} \end{matrix} \right\} \tag{11}$$

Constraints (7)-(8) represent the uncertainty output power of RES $\tilde{P}^{\mathrm{W}}_{w,t,s}$ and the uncertainty load demand $\tilde{P}^{\mathrm{L}}_{i,t,s}$. Constraint (9) represents the total uncertainty degree of different nodes, which includes both the uncertainty of RES at node *i* and the uncertainty of load demand at node *i*. The maximum /minimum uncertainty value of node *i* is obtained in (10)-(11), where $\tilde{\Delta}^{\max}_{i,t,s}$ and $\tilde{\Delta}^{\max}_{i,t,s}$ represent the maximum and minimum uncertainty degree of node *i*.

Then, the second max in the lower level uses the ARO method to address the seasonal uncertainty of RES. ARO introduces adjustable variables in operation decision stage, aiming to find the optimal safe operation solution to avoid the possible constraints violation under the worst case of seasonal uncertainty set. The adjustable variables represent "wait-and-see" decisions which can adjust themselves to actual RES output power in different seasons. The specific modeling process of ARO is described in Section IV.

III. Tri-level Planning Model Formulation

A. Objective function of the proposed tri-level model

The objective function (12) of the proposed tri-level model is to minimize the sum of annual HES investment costs and operation costs under the worst-case of long-term and seasonal uncertainty sets, which are shown in (13)-(20).

$$\min_{\mathbf{x}} C_{\mathrm{inv}} + \max_{\tilde{p}_n \in \mathcal{P}} \{ \sum_{n \in \mathcal{N}} \tilde{p}_n [\max_{\tilde{\Delta} \in \mathcal{U}} \min_{\mathbf{y}} \varsigma \sum_{s \in \mathcal{S}} p_s C_{\mathrm{ope}}(s)] \} \tag{12}$$

$$C_{\mathrm{inv}} = C^{\mathrm{E}}_{\mathrm{inv}} + C^{\mathrm{P}}_{\mathrm{inv}} \tag{13}$$

$$C^{\mathrm{E}}_{\mathrm{inv}} = CRF \cdot C_{\mathrm{E}} \sum_{i \in \mathcal{I}} x_i \frac{H_l S_i}{LHV} \tag{14}$$

$$C^{\mathrm{P}}_{\mathrm{inv}} = CRF \cdot C^{\mathrm{FC}}_{\mathrm{P}} \sum_{i \in \mathcal{I}} x_i S_i + CRF \cdot C^{\mathrm{P2H}}_{\mathrm{P}} \sum_{i \in \mathcal{I}} x_i S_i \tag{15}$$

$$CRF = \frac{r(1+r)^{T_x}}{(1+r)^{T_x} - 1} \tag{16}$$

$$C_{\mathrm{ope}}(s) = C_{\mathrm{w}}(s) + C_{\mathrm{g}}(s) + C_{\mathrm{u}}(s) \tag{17}$$

$$C_{\mathrm{w}}(s) = \sum_{t \in \mathcal{T}} \sum_{w \in \mathcal{N}^{\mathcal{RS}}} c_w P^{\mathrm{W}'}_{w,t,s,n} + \sum_{t \in \mathcal{T}} \sum_{i \in \mathcal{I}} c_i P^{\mathrm{Load}'}_{i,t,s,n} \tag{18}$$

$$C_{\mathrm{g}}(s) = \sum_{t \in \mathcal{T}} \sum_{g \in \mathcal{N}^{\mathcal{TG}}} c_g P^{\mathrm{G}}_{g,t,s,n} \tag{19}$$

$$C_{\mathrm{u}}(s)=\sum_{t\in\mathcal{T}}\sum_{g\in\mathcal{N}^{\mathcal{TG}}}\left(c_g^{\mathrm{su}}U_{g,t,s,n}+c_g^{\mathrm{sd}}D_{g,t,s,n}\right) \quad (20)$$

The investment costs include storage devices and power devices cost, which is shown as (13). Equation (14) calculates the investment cost of HT. Equation (15) calculates investment costs of P2H and FC. Equation (16) is the capital recovery factor to calculate annual investment cost based on the device lifetime $\mathbb{T}_x$. The operation costs of typical day s under typical long-term RES scenario n consist of RES and load curtailment penalty cost, thermal generation fuel cost and thermal generation start-up/shut-down cost, which are calculated in (18)-(20), respectively. ς is the conversion coefficient of equivalent annual cost and p_s is the probability of typical day scenario s under representative RES scenario n.

B. Constraints of the proposed tri-level model

1) HES planning and investment constraints: HES planning and investment constraints limit HES number and capacity. Specifically, constraint (21) limits the number of HESs allowed to be installed, where N_{HES} is the maximum planning numbers for HES. Constraints (22) limits the P2H and FC capacity installed at node i.

$$\sum_{i\in\mathcal{I}}x_i\le N_{\mathrm{HES}} \quad (21)$$

$$x_i\,Cap_i^{\min}\le S_i\le x_i\,Cap_i^{\max} \quad (22)$$

2) HES operation constraints: HES storage operation constraints are modelled as (23)-(31) according to [3], [18]. The SOC of HES is decomposed into inter-day and intra-day component in (23). Intra-day constraint in (24) describes SOC relationship during the typical intraday period to reduce computational burden where η is the efficiency of charging/discharging, while inter-day constraints in (25) describe SOC relationship between adjacent natural days to keep SOC continuity in a whole yearly cycle. Equation (26) limits the initial value of intra-day SOC should be equal to 0. Equation (27) is the energy balance constraint of HES in a yearly cycle, which limits the SOC of initial and final state should be equal. Equation (28) limits the charge power of P2H cannot exceed the planning capacity. To address RES seasonal uncertainty, HES needs to provide a certain reserve capacity. Equations (29)-(30) limit that the discharge power and reserve capacity of HES cannot exceed the planning capacity. Equation (31) limits the lower and upper hydrogen stored in HES, $\mathrm{SOC}_{\min}$ and $\mathrm{SOC}_{\max}$ are set as 0.05 and 0.95 similar to battery storage for safety purpose. H_l is the duration time of HES (720 hours in this paper) [3] and LHV is the low heating value of hydrogen (kWh/kg H_2).

$$SOC_{i,t,d,n}=SOC_{i,d,n}^{\mathrm{inter}}+SOC_{i,t,s=\varpi(d),n}^{\mathrm{intra}} \quad (23)$$

$$SOC_{i,t+1,s=\varpi(d),n}^{\mathrm{intra}}=SOC_{i,t,s=\varpi(d),n}^{\mathrm{intra}}+\left\{\frac{\eta^{\mathrm{Cha}}P_{i,t,s=\varpi(d),n}^{\mathrm{P2H,Cha}}}{LHV}-\left(\frac{P_{i,t,s=\varpi(d),n}^{\mathrm{FC,Dis}}+P_{i,t,s=\varpi(d),n}^{\mathrm{FC,r}}}{\eta^{\mathrm{Dis}}LHV}\right)\right\} \quad (24)$$

$$SOC_{i,d+1,n}^{\mathrm{inter}}=SOC_{i,d,n}^{\mathrm{inter}}+SOC_{i,\mathrm{T},s=\varpi(d),n}^{\mathrm{intra}} \quad (25)$$

$$SOC_{i,1,s=\varpi(d),n}^{\mathrm{intra}}=0 \quad (26)$$

$$SOC_{i,1,n}^{\mathrm{inter}}=SOC_{i,\mathrm{D},n}^{\mathrm{inter}} \quad (27)$$

$$0\le P_{i,t,s=\varpi(d),n}^{\mathrm{P2H,Cha}}\le S_i \quad (28)$$

$$P_{i,t,s=\varpi(d),n}^{\mathrm{FC,Dis}}+P_{i,t,s=\varpi(d),n}^{\mathrm{FC,r}}\le S_i \quad (29)$$

$$P_{i,t,s=\varpi(d),n}^{\mathrm{FC,Dis}}-P_{i,t,s=\varpi(d),n}^{\mathrm{FC,r}}\ge 0 \quad (30)$$

$$\mathrm{soc}_{\min}H_lS_i\le LHV\cdot SOC_{i,t,d,n}\le \mathrm{soc}_{\max}H_lS_i \quad (31)$$

HES has cross-season regulation, so the consideration of a whole yearly SOC cycle is essential. As Fig. 4 shows, based on the representative RES scenarios with 8760-hour output power series and the affine relationship, the intra-day hourly operation is considered within typical days, which are obtained by scenarios reduction technology [26]. The inter-day daily operation is considered in the natural days, and the intra-day hourly operation constraints of different natural days can be described by the typical days, where ϖ describes the affine relationship function of natural day d to typical day s. For example, if Day 2 and Day 4 are classified into the cluster of typical day scenario S_1, and then HES operation constraints are decomposed into inter-day component $SOC_{i,2,n}^{\mathrm{inter}}$, $SOC_{i,4,n}^{\mathrm{inter}}$ and intra-day component $SOC_{i,t,1,n}^{\mathrm{intra}}$, which reduce the computational burden and simulate the continuity dynamic behaviour of hydrogen storage in a whole yearly cycle.

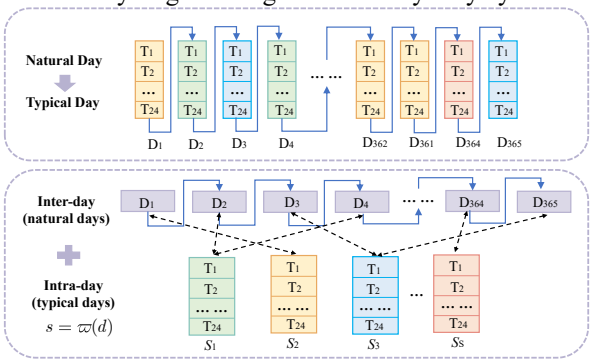

Fig. 4. The SOC of HES modelling illustration.

3) Thermal power unit commitment constraints: Thermal power units should also provide reserve capacity to address RES seasonal uncertainty. Thermal power unit commitment should meet ramping limit, maximum/minimum power output limit, and on/off limit. Equations (32)-(33) limit the lower and upper output of thermal power unit g. Equations (34)-(35) are ramping constraints of thermal power unit g. Equations (36)-(37) formulate up and down state constraints of thermal power unit g. Equations (38)-(39) limit the minimum on/off time $T_{on,g}$ / $T_{off,g}$ of thermal power unit g, respectively.

$$P^{\mathrm{G}}_{g,t,s,n} + P^{\mathrm{G,r}}_{g,t,s,n} \le I_{g,t,s,n} P^{\max}_{g} \tag{32}$$

$$P^{\mathrm{G}}_{g,t,s,n} - P^{\mathrm{G,r}}_{g,t,s,n} \ge I_{g,t,s,n} P^{\min}_{g} \tag{33}$$

$$P^{\mathrm{G}}_{g,t+1,s,n} - P^{\mathrm{G}}_{g,t,s,n} \le R^{\mathrm{U}}_{g} I_{g,t,s,n} + R^{\mathrm{SU}}_{g} U_{g,t,s,n} \tag{34}$$

$$P^{\mathrm{G}}_{g,t,s,n} - P^{\mathrm{G}}_{g,t+1,s,n} \le R^{\mathrm{D}}_{g} I_{g,t+1,s,n} + R^{\mathrm{SD}}_{g} D_{g,t,s,n} \tag{35}$$

$$U_{g,t,s,n} + D_{g,t,s,n} \le 1 \tag{36}$$

$$U_{g,t,s,n} - D_{g,t,s,n} = I_{g,t+1,s,n} - I_{g,t,s,n} \tag{37}$$

$$\sum_{\tau=t+1}^{t+T_{\mathrm{on},g}} I_{g,\tau,s,n} \ge T_{\mathrm{on},g} U_{g,t,s,n} \tag{38}$$

$$\sum_{\tau=t+1}^{t+T_{\mathrm{off},g}} (1 - I_{g,\tau,s,n}) \ge T_{\mathrm{off},g} D_{g,t,s,n} \tag{39}$$

4) Power system operational constraints: The power system operation should meet power flow and power balance constraints. Equation (40) formulates the power balance of node *i* at time *t* under typical day *s*. Equation (41) calculates the power flow of transmission line *l* at time *t* under typical day *s* based on the DC power flow. Equations (42)-(43) limit the lower/upper power flow of line *l* and angle of node *i*, respectively.

$$\begin{aligned}&(P^{\mathrm{W}}_{w,t,s,n} - P^{\mathrm{W}'}_{w,t,s,n}) + (P^{\mathrm{FC,Dis}}_{i,t,s,n} - P^{\mathrm{P2H,Cha}}_{i,t,s,n}) + P^{\mathrm{G}}_{g,t,s,n} \\ &+ \sum_{l \in \Omega^{LE}_{i}} P_{l,t,s,n} - \sum_{l \in \Omega^{LS}_{i}} P_{l,t,s,n} = P^{\mathrm{Load}}_{i,t,s,n} - P^{\mathrm{Load}'}_{i,t,s,n}\end{aligned} \tag{40}$$

$$P_{l,t,s,n} = \Big(\sum_{i \in \Omega^{LS}_{l}} \theta_{i,t,s,n} - \sum_{j \in \Omega^{LE}_{l}} \theta_{j,t,s,n}\Big) / \, x_l \tag{41}$$

$$-P^{\max}_{l} \le P_{l,t,s,n} \le P^{\max}_{l} \tag{42}$$

$$\theta^{\min}_{i} \le \theta_{i,t,s,n} \le \theta^{\max}_{i} \tag{43}$$

5) Carbon emission limit constraints: To meet the needs of low-carbon development, thermal power units need to meet carbon emission limit [29]. Specifically, constraint (44) limits the total carbon emission of thermal power unit should not exceed the total carbon emission rights CER, where o_g is the emission coefficient of thermal power unit *g*.

$$\sum_{g \in \mathcal{N}^{\mathcal{TG}}} \sum_{t \in \mathcal{T}} o_g (P^{\mathrm{G}}_{g,t,s,n} + P^{\mathrm{G,r}}_{g,t,s,n}) \le CER \tag{44}$$

6) Robust constraints: to address the seasonal uncertainty of RES, thermal power unit and HES provide a certain amount of reserve capacity. The participation factor method [30] is used to optimize reserve capacity. Equation (45) formulates the sum of participation factors of node *i* should be equal to 1. Constraint (46) limits the range of participation factor belong to [0,1]. Equations (47)-(48) suggest thermal power unit and HES must provide a certain amount of reserve capacity to meet the seasonal uncertainty ($\forall \tilde{\Delta}_{i,t,s,n} \in [\tilde{\Delta}^{\min}_{i,t,s,n}, \tilde{\Delta}^{\max}_{i,t,s,n}]$). A^{g}_{i} is the element of thermal generation unit-node incidence matrix.

$$\sum_{i \in \mathcal{I}} \lambda^{\mathrm{FC}}_{i,t,s,n} + \sum_{i \in \mathcal{I}} \lambda^{\mathrm{G}}_{i,t,s,n} = 1 \tag{45}$$

$$0 \le \lambda^{\mathrm{FC}}_{i,t,s,n}, \lambda^{\mathrm{G}}_{i,t,s,n} \le 1 \tag{46}$$

$$-\sum_{g \in \mathcal{N}^{\mathcal{TG}}} A^{g}_{i} P^{\mathrm{G,r}}_{g,t,s,n} \le \lambda^{\mathrm{G}}_{i,t,s,n} \sum_{i \in \mathcal{I}} \tilde{\Delta}_{i,t,s,n} \le \sum_{g \in \mathcal{N}^{\mathcal{TG}}} A^{g}_{i} P^{\mathrm{G,r}}_{g,t,s,n} \tag{47}$$

$$-P^{\mathrm{FC,r}}_{i,t,s,n} \le \lambda^{\mathrm{FC}}_{i,t,s,n} \sum_{i \in \mathcal{I}} \tilde{\Delta}_{i,t,s,n} \le P^{\mathrm{FC,r}}_{i,t,s,n} \tag{48}$$

IV. Solution Procedure and Algorithm

In this section, the solution procedure of the proposed hybrid tri-level DRO-ARO model by using the improved C&CG algorithm by leveraging adaptive robust reformulation alongside parallel computation of duality-free decomposition method is presented. C&CG algorithm terminates in a finite number of iterations, which has been proved in [31]. The final model is a MILP problem, which can be expressed in a compact form as bellows:

$$\min_{\mathbf{x}} C_{\mathrm{inv}} + \max_{\tilde{p}_n \in \mathcal{P}} \{ \sum_{n \in \mathcal{N}} \tilde{p}_n [\max_{\tilde{\Delta} \in \mathcal{U}} \min_{\mathbf{y}} \varsigma \sum_{s \in \mathcal{S}} p_s C_{\mathrm{ope}}(s)] \} \tag{49}$$

$$s.t.\ \mathbf{Ax} \le \mathbf{b} \tag{50}$$

$$\tilde{\mathbf{p}} \le \mathbf{D}\xi \tag{51}$$

$$\mathbf{Ex} + \mathbf{Fy} \le \mathbf{g} \tag{52}$$

$$\mathbf{Hx} + \mathbf{Iy} + \mathbf{J}\tilde{\mathbf{u}} \le \mathbf{q} \tag{53}$$

where equation (50) represents HES planning constraints including (21)-(22); Equation (51) represents RES long-term uncertainty constraints including (2)-(6); Equation (52) represents the operation constraints including (23)-(44). Equation (53) represents robust constraints (7)-(11), (45)-(48) to address the seasonal uncertainty of RES.

A. ARO Reformulation

The hybrid tri-level structure is one of the reasons making the proposed model difficult to be solved. Therefore, firstly, the ARO method is used to reformulate the lower-level uncertain problem caused by RES seasonal uncertainty as a deterministic model. Robust constraints seek to optimize adjustable variables to minimize operation cost and ensure the corresponding constraints can always be satisfied for any realization of uncertainties [32]. In this paper, adjustable variables include reserve capacity of thermal power unit $P^{\mathrm{G,r}}_{g,t,s,n}$ and HES $P^{\mathrm{FC,r}}_{i,t,s,n}$. The reformulation steps of robust constraints can be summarized as two steps [30]: a) Identify the "worst-case" where uncertainties are most likely to invalidate the robust constraints; b) Substitute the original constraints with constraints where the uncertainties are fixed as these "worst-case" values. In this paper, the robust constraints to address RES seasonal uncertainty include (47)-(48). Detailed reformulation process for (47)-(48) is shown as bellow:

1) For constraint (47)

Robust constraint (47) means that for any realization of uncertainties $\forall \tilde{\Delta}_{i,t,s,n} \in [\tilde{\Delta}^{\min}_{i,t,s,n}, \tilde{\Delta}^{\max}_{i,t,s,n}]$, there always exists an adjustable variable $P^{\mathrm{G,r}}_{g,t,s,n}$ for which (47) is satisfied. Therefore, the constraint (47) can be reformulated as follows:

$$\begin{cases} -\sum_{g\in\mathcal{N}^{\mathcal{TG}}} A_i^g P_{g,t,s,n}^{\mathrm{G,r}} - \lambda_{i,t,s,n}^{\mathrm{G}} \sum_{i\in\mathcal{I}} \tilde{\Delta}_{i,t,s,n} \le 0, \forall \tilde{\Delta}_{i,t,s,n} \in [\tilde{\Delta}_{i,t,s,n}^{\min}, \tilde{\Delta}_{i,t,s,n}^{\max}] \\ -\sum_{g\in\mathcal{N}^{\mathcal{TG}}} A_i^g P_{g,t,s,n}^{\mathrm{G,r}} + \lambda_{i,t,s,n}^{\mathrm{G}} \sum_{i\in\mathcal{I}} \tilde{\Delta}_{i,t,s,n} \le 0, \forall \tilde{\Delta}_{i,t,s,n} \in [\tilde{\Delta}_{i,t,s,n}^{\min}, \tilde{\Delta}_{i,t,s,n}^{\max}] \end{cases} \tag{54}$$

$$\begin{cases} -\sum_{g\in\mathcal{N}^{\mathcal{TG}}} A_i^g P_{g,t,s,n}^{\mathrm{G,r}} - \lambda_{i,t,s,n}^{\mathrm{G}} \sum_{i\in\mathcal{I}} \tilde{\Delta}_{i,t,s,n}^{\min} \le 0 \\ -\sum_{g\in\mathcal{N}^{\mathcal{TG}}} A_i^g P_{g,t,s,n}^{\mathrm{G,r}} + \lambda_{i,t,s,n}^{\mathrm{G}} \sum_{i\in\mathcal{I}} \tilde{\Delta}_{i,t,s,n}^{\max} \le 0 \end{cases} \tag{55}$$

In constraint (55), uncertainty variables $\tilde{\Delta}_{i,t,s,n}$ are fixed as the "worst-case" values to ensure robust constraint can be satisfied under the worst case by adjustable variable $P_{g,t,s,n}^{\mathrm{G,r}}$.

2) For constraint (48)

Similarly, the reformulation of (48) by the ARO method can be written as (56).

$$\begin{cases} -P_{i,t,s,n}^{\mathrm{FC,r}} - \lambda_{i,t,s,n}^{\mathrm{FC}} \sum_{i\in\mathcal{I}} \tilde{\Delta}_{i,t,s,n}^{\min} \le 0 \\ -P_{i,t,s,n}^{\mathrm{FC,r}} + \lambda_{i,t,s,n}^{\mathrm{FC}} \sum_{i\in\mathcal{I}} \tilde{\Delta}_{i,t,s,n}^{\max} \le 0 \end{cases} \tag{56}$$

After ARO reformulation, the lower-level seasonal uncertainty problem is transferred into a deterministic model. Finally, the proposed tri-level model (49) is reformulated by ARO as (57)-(61), where the robust constraint (61) includes (7)-(11), (47)-(48) are replaced as (55)-(56).

$$\min_{\mathbf{x}} C_{\mathrm{inv}} + \max_{\tilde{p}_n\in\mathcal{P}} \{ \sum_{n\in\mathcal{N}} \tilde{p}_n [\min_{\mathbf{y}} \varsigma \sum_{s\in\mathcal{S}} p_s C_{\mathrm{ope}}(s)] \} \tag{57}$$

$$s.t.\ \mathbf{Ax} \le \mathbf{b} \tag{58}$$

$$\tilde{\mathbf{p}} \le \mathbf{D}\xi \tag{59}$$

$$\mathbf{Ex} + \mathbf{Fy} \le \mathbf{g} \tag{60}$$

$$\mathbf{Hx} + \mathbf{Iy} + \mathbf{Ku}_{\max} + \mathbf{Lu}_{\min} \le \mathbf{q} \tag{61}$$

B. C&CG Algorithm

For solving the reformulation model (57)-(61), C&CG algorithm can decompose the primal problem into the upper main problem and the lower subproblem [31]. The upper main problem is to optimize HES planning decisions by minimizing the investment costs under the known scenario's probability. With a dummy auxiliary variable η, the main problem can be expressed as (62). The main problem is a relaxation problem of the primal problem, providing the lower bound LB for the primal problem. Mathematically, it is a standard MILP model and can be easily solved by the commercial solvers.

$$\begin{aligned} MP\text{:}\ & \min_{\mathbf{x}} C_{\mathrm{inv}} + \eta \\ \text{s.t.}\ & \begin{cases} \mathbf{Ax} \le \mathbf{b} \\ \mathbf{Ex} + \mathbf{Fy}^l \le \mathbf{g}, \forall l \le m \\ \mathbf{Hx} + \mathbf{Iy}^l + \mathbf{Ku}_{\max} + \mathbf{Lu}_{\min} \le \mathbf{q}, \forall l \le m \\ \eta \ge \sum_{n=1}^{N} \tilde{p}_n^l [\varsigma \sum_{s=1}^{S} p_s C_{\mathrm{ope}}^l(s)], \forall l \le m \end{cases} \end{aligned} \tag{62}$$

After solving the upper main problem, HES planning results are obtained. Under a given planning scheme, the lower subproblem is to find the worst probability distribution and optimize operation strategy to minimize system operation cost.

Different from the traditional lower subproblem with "max-min" bi-level structure that needs the dual transformation of inner level "min" problem to realize solution [31], the proposed model does not need to dualize the inner model when solving the bi-level subproblem, which is referred to duality-free decomposition method [33]. Specifically, the uncertain probability distribution of RES scenarios and system operation variables are independent with each other. Therefore, the lower level subproblem can be further decoupled into subproblem SP1 (63) and subproblem SP2 (64).

$$\begin{aligned} \mathrm{SP1}:\ & \min_{\mathbf{y}} f(n) = \varsigma \sum_{s=1}^{S} p_s C_{\mathrm{ope}}(s) \\ & \text{s.t. } (23)\text{-}(46), (55)\text{-}(56) \end{aligned} \tag{63}$$

$$\begin{aligned} \mathrm{SP}_2\text{:}\ & \max_{\tilde{p}_n\in\mathcal{P}} \sum_{n=1}^{N} \tilde{p}_n f(n) \\ & \text{s.t. } (2)-(6) \end{aligned} \tag{64}$$

Since representative RES scenarios under different climate conditions are independent with each other, subproblem 1 can be solved in parallel and then transmits operation costs to subproblem 2 to calculate the worst probability distribution of RES scenarios with the largest operation costs. After completing the solution of lower subproblem by solving SP1 and SP2, a set of representative scenarios' probability distribution will be generated, which returns to the upper main problem to update HES planning scheme in the next iteration, so subproblem provides an upper bound UB for solution.

The complete solution procedure for the proposed hybrid tri-level DRO-ARO model is described as **Algorithm1**.

Algorithm1 Improved duality-free decomposition C&CG algorithm

Step 1 Initialization:

Set $m = 0, LB = -\infty, UB = +\infty$

Step 2 ARO reformulation:

Identify the "worst-case" for (47)-(48), $\tilde{\Delta}_{i,t,s,n} \in [\tilde{\Delta}_{i,t,s,n}^{\min}, \tilde{\Delta}_{i,t,s,n}^{\max}]$

Fix $\tilde{\Delta}_{i,t,s,n}$ as the "worst-case" values, substitute (47)-(48) with (55)-(56).

Step 3 Solve the upper master problem (62) and update LB:

$LB = C_{\mathrm{inv}} + \eta$

Obtain $\mathbf{x}$

Step 4 Solve the lower subproblem SP1 (63) and SP2 (64) by duality-free decomposition solving method, update UB:

$$UB = \min\{UB, C_{\mathrm{inv}} + \sum_{n=1}^{N} \tilde{p}_n [\varsigma \sum_{s=1}^{S} p_s C_{\mathrm{ope}}(s)]\}$$

Step 5 Termination:

If $\varepsilon^{m+1} = (UB - LB) / LB \le \mathrm{gap}$: Stop and return $\mathbf{x}$

Else update *m*=*m*+1 and go to Step 3, add the cuts:

$$\eta \ge \sum_{n=1}^{N} \tilde{p}_n^l [\varsigma \sum_{s=1}^{S} p_s C_{\mathrm{ope}}^l(s)], \forall l \le m$$

VI. Case Studies

The proposed tri-level HES planning model and solution approach are validated on modified IEEE 39-bus and IEEE 118-bus test systems. All simulations are conducted using MATLAB 2020b and YALMIP on a PC equipped with an Intel Octa-Core processor (3.0 GHz) and 16 GB of RAM. The MILP problems are solved using Gurobi 11.0 under an academic license with default solver settings.

TABLE I
BASIC PARAMETERS SETTING

Parameter	Value
c_g	40 \$/MWh
c_w / c_i	300 \$/MWh / 600 \$/MWh
C_P^{P2H} / C_P^{FC}	320000 \$/MW
C_E	30 \$/kg H_2
N_{HES}	12

The basic parameters are shown in Table I. The min/max capacity $Cap_i^{\min}$ / $Cap_i^{\max}$ of P2H and FC for installation are 10/200 MW. Discount ratio of investment r is set as 10%. Investment payback years of HT, P2H and FC are 25 years, 10 years and 10 years. The seasonal fluctuation parameters of wind power are set as ±8% for spring and winter and ±5% for summer and autumn. The seasonal fluctuation parameters of PV power are set as ±8% for spring and summer and ±5% for autumn and winter.

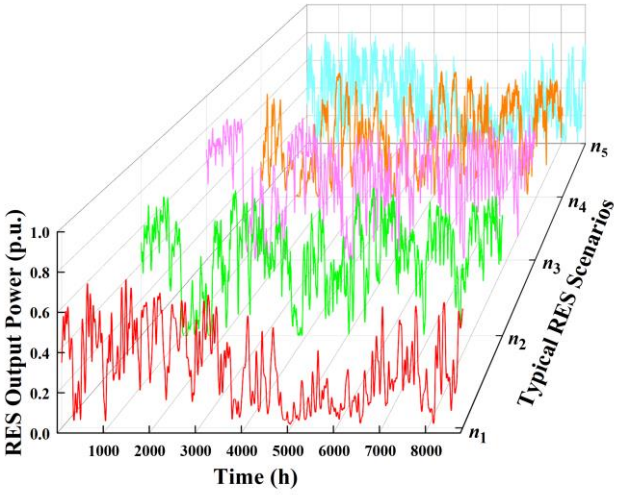

Fig. 5. Five representative RES scenarios after reduction.

Five representative RES scenarios after reduction are shown in Fig. 5, which are obtained based on the data characteristics of 100 RES scenarios generated according to the RES historical dataset from 2014-2023. The seasonal and trend component is captured using STL algorithm for HES planning. Seasonal and trend component of representative RES scenario n_1 is shown in Fig. 6. RES output power is smoother than the original curve after capturing the seasonal fluctuation characteristics by the STL algorithm. The pink area of Fig. 6 is the seasonal uncertainty range of representative RES scenario n_1 throughout the year. Then, the obtained seasonal and trend component is clustered into 16 typical day scenarios over four seasons [28].

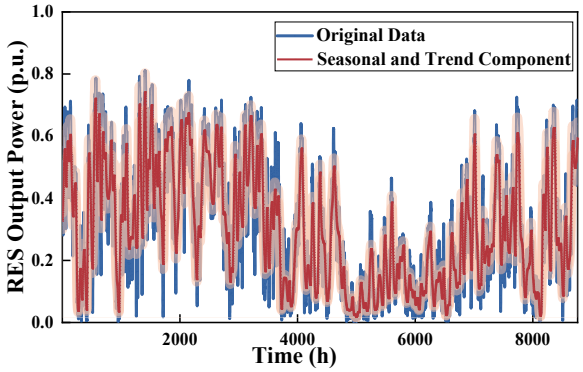

Fig. 6. Seasonal and trend component of RES scenario n_1.

A. IEEE 39-bus test system

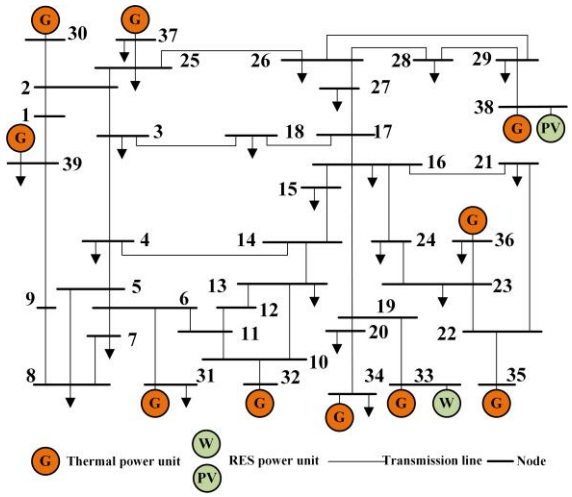

Fig. 7. IEEE 39-bus test system.

1) Numerical Description: the modified IEEE 39-bus test system is shown in Fig. 7, including ten thermal power units, two RES units (one wind unit and one PV unit). The total capacity of thermal power units is 6000MW and the total capacity of RES is 800MW. More details about IEEE 39-bus test system and start-up/shut-down costs of the thermal generators can be found in [34].

TABLE II
HES PLANNING RESULTS.

Node	P2H/FC (MW)	HT (t H_2)
17	39.41	945.81
19	88.15	2115.57
30	100.20	2404.89
Total	227.76	5466.27

2) Simulation Results: The planning results of HES on IEEE 39-bus test system are presented in Table II. P2H/FC units are deployed at three nodes, with a total installed capacity of 227.76 MW. The total HT capacity reaches 5466.27t H_2. In addition, a whole yearly SOC curve of HT under the representative RES scenario n_1 is shown in Fig. 8. SOC curve shows that hydrogen storage behavior and HES charge/discharge strategy is influenced by RES seasonal fluctuations. HES operates in shorter cycles in spring (min 2384t and max 5058t H_2 from 0 to 2190 h) and summer (min 3037t and max 5068t H_2 from 2190 to 4380h). Due to the rich output of RES in summer, SOC shows an overall upward trend

with 2031t H_2 increased. In addition, HES charges/discharges slightly and frequently due to RES fluctuations, especially in summer. In autumn (4380-6570h) and winter (6570-8760h), HES operates in long cycles, ranging from min 275t to max 5192t H_2. In autumn, HES discharges deeply and continuously due to the low output of RES. To keep yearly SOC balance, HES charges continuously and SOC shows an upward trend in winter, from 275t to 5192t H_2. Moreover, HES is also helpful to some extreme cases. For example, RES is in extreme low output (less than 1%) from 3708 to 3740h, which is shown in red mark circle in Fig. 8, HES keeps a long continuous release state to address imbalance between supply and demand.

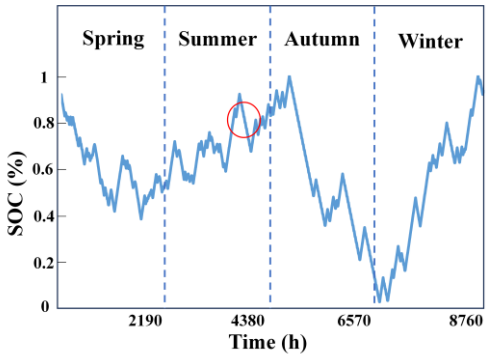

Fig. 8. The whole year SOC curve of HT in IEEE 39-bus test system for representative RES scenario n_1.

3) Impact of long-term seasonal uncertainty: In this paper, DRO is utilized to address RES long-term uncertainty impacted by climate variability. Specifically, the probability distribution ambiguity set of RES scenarios is constructed using norm constraints. The ambiguity set can guarantee to cover all possible probability distributions under a given confidence level γ. The influence of γ on the HES planning results is shown in Fig. 9. The total costs increase from 1.6806*10^9\$ to 1.6820*10^9\$ with the confidence level γ increases from 0.6 to 0.99. When γ is from 0.6 to 0.8, the total costs increase 0.4*10^6\$. While the total costs increase 1.0*10^6\$ with γ from 0.8 to 0.99. This is because a large value of γ means that the RES uncertainty is higher, hence a higher capacity of HES is needed to address RES long-term uncertainty. Therefore, a reasonable value of γ is essential to ensure HES planning results adapt to the long-term uncertainty of RES.

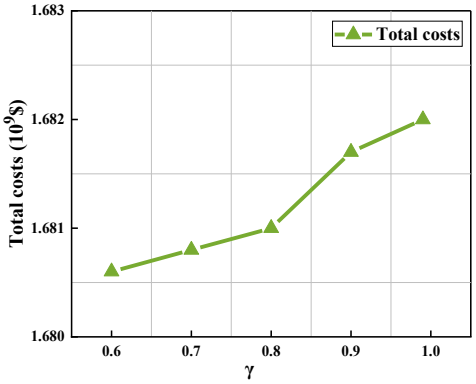

Fig. 9. Total costs under different confidence level.

Moreover, to analyze the impact of seasonal uncertainty on operation strategy, the hourly output power of different units in four typical days across different seasons is shown in Fig. 10. In this paper, ARO is utilized to address RES seasonal uncertainty. The uncertainty set of RES seasonal uncertainty is constructed according to RES prediction error distributions in different seasons. It can be found that the reserve capacity (red coding is reserve from thermal generation and cyan coding is reserve from HES) is higher in spring due to the high uncertainty of RES, and the reserve capacity in summer is low. Moreover, RES output power is poor in autumn, so the discharging power of HES is higher while the charging power (blue coding in Fig. 10) is lower. Notably, the charging power of HES $P^{\mathrm{P2H,Cha}}$ is plotted as a negative value to visually represent the charging behavior (electricity consumption for hydrogen production by P2H). While in the model formulation $P^{\mathrm{P2H,Cha}}$ is defined as a non-negative variable to represent the magnitude of HES charging power, it is displayed as negative in the Fig. 10 purely for visualization purposes. During winter and summer, the charging power of HES is higher due to the abundant output of RES. So, seasonal regulation of RES can be realized by reasonable planning of HES in power systems.

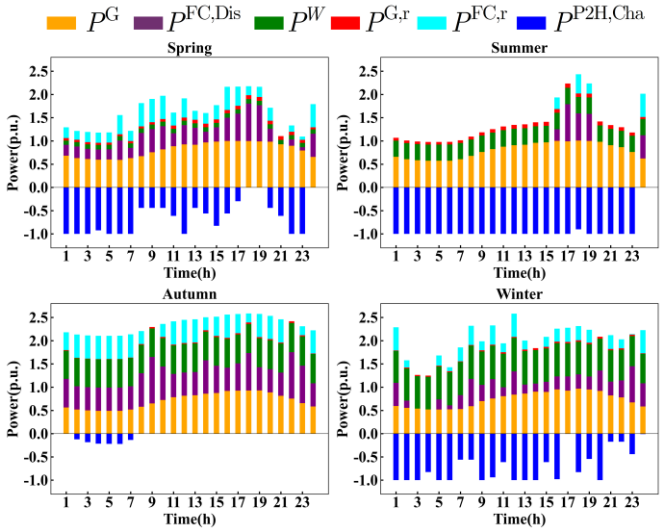

Fig. 10. Hourly power output of units in four typical days across different seasons.

B. IEEE 118-bus test system

1) Numerical Description: to further validate the effectiveness of the proposed method on large-scale systems, we also test the proposed method on the modified IEEE 118-bus test system. Fig. 11 shows the topology of the modified IEEE 118-bus test system [35] which consists of 54 thermal power units, 6 RES units (3 wind units and 3 PV units). The total capacity of thermal power units is 9960MW and the total capacity of RES is 4200MW. The five representative RES scenarios of 8760 hours used for planning are as the same as per-unit output profiles shown in Fig. 5.

2) Simulation Results: The HES planning results on the modified IEEE 118-bus test system are summarized in Table III, which shows the total deployment of P2H/FC at 11 nodes.

The total installed capacity of P2H and FC reaches 2082.6 MW, with the total HT capacity of 49982.4t H_2.

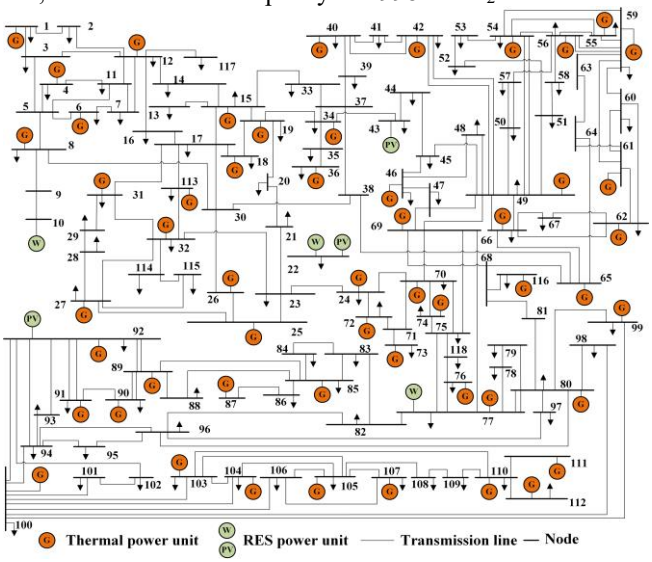

Fig. 11. IEEE 118-bus test system.

TABLE III
HES PLANNING RESULTS.

Node	P2H/FC (MW)	HT (t H_2)
3	200.0	4800.0
10	82.6	1982.4
11	200.0	4800.0
23	200.0	4800.0
34	200.0	4800.0
46	200.0	4800.0
65	200.0	4800.0
73	200.0	4800.0
75	200.0	4800.0
89	200.0	4800.0
94	200.0	4800.0
Total	2082.6	49982.4

AS shown in Fig. 12, the SOC curve of HT in IEEE 118-bus system for five representative RES scenarios further clearly reflect the operation strategy of HES system is strongly influenced by the seasonal fluctuations of RES and demonstrate the seasonal energy-shifting capability of HES in response to RES seasonal fluctuations. Across the five representative RES scenarios, significant seasonal change in RES output is particularly observed in scenario n_1 and n_5, lower availability of RES is during autumn. Correspondingly, the SOC trajectories show continuous decline during these periods, indicating sustained discharge via FC to support system demand. In contrast, during high-output seasons such as summer and winter, excess RES is utilized for hydrogen production via P2H units, leading to a gradual increase in SOC. This pattern demonstrates the seasonal energy-shifting capability of the HES system, where hydrogen serves as a long-term storage medium that bridges the temporal mismatch between RES supply and load demand. Such seasonal balancing not only enhances supply adequacy during critical periods but also reduces the reliance on conventional backup generation. Additionally, in scenarios n_2, n_3 and n_4 (especially during autumn and winter), the RES output shows more frequent fluctuations. In response, the HES system displays more dynamic and frequent charge/discharge cycles, reflecting its flexible operational strategy in coping with RES fluctuations.

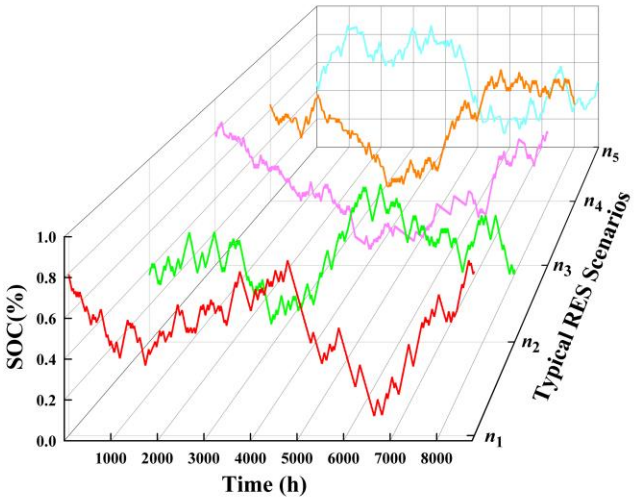

Fig. 12. The whole year SOC curve of HT in IEEE 118-bus test system for five representative RES scenarios.

In addition to its function in seasonal regulation and addressing RES fluctuations, HES also plays a critical role in handling extreme climate scenarios characterized by prolonged renewable scarcity, such as long periods with low wind and solar irradiance. For example, from 1009 h to 1082 h of representative RES scenario n_2, the RES output drops to an extremely low level, representing a typical climate case of long-duration "no-wind-and-little-sunshine" conditions. As shown in Fig. 13, HES enters a continuous discharge state throughout this period, delivering sustained and reliable power to bridge the severe supply-demand gap. This demonstrates the function of HES in enhancing system resilience, enabling it to stably support the grid through extreme renewable droughts where short-duration storage or flexible generation alone would be insufficient under high-RES penetrations.

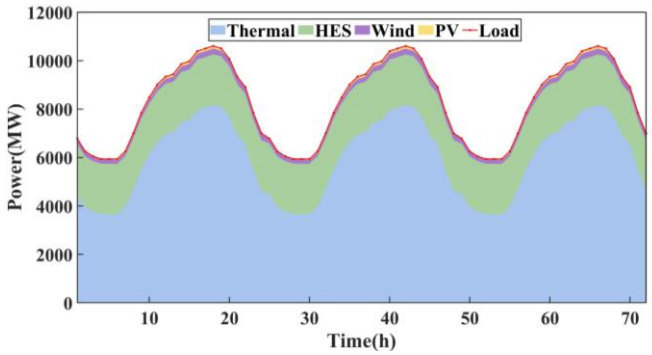

Fig. 13. Hourly power balance from 1009h to 1082h of representative RES scenario n_2.

3) Impact of RES penetration and HES investment cost: in this section, the impact of different factors including RES penetration and unit HES investment cost on the planning

decisions are analyzed and the corresponding results are illustrated in Fig. 14.

As illustrated in Fig. 14, the optimal rated power of HES increases significantly with higher RES penetration, rising from 2603 MW at 30% penetration to 5727 MW at 70% penetration under a low investment cost scenario, indicating a greater need for storage capacity to address RES fluctuations and ensure supply-demand balance under high-RES scenarios. Conversely, as the investment cost rises, the optimal storage capacity decreases, reflecting the influence of economic considerations on planning decisions. For instance, at 30% RES penetration, Prated drops from 2603 MW (low cost) to 1874 MW (high cost). Moreover, the contour lines further reveal that in regions with high-RES penetration and low investment cost, the optimal rated power of HES is more sensitive to parameter variations. This figure highlights the relationship between RES integration and energy storage investment, offering quantitative insights for optimal planning.

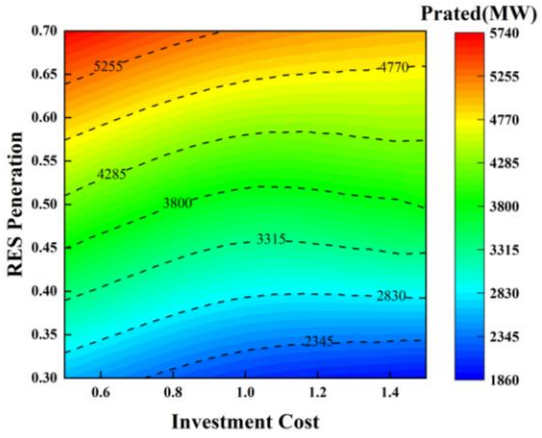

Fig. 14. HES planning results of IEEE 118-bus test system under different factors.

C. Comparative Analysis

1) Comparison results: to analyze RES long-term seasonal uncertainties on HES planning results, four cases including the existing methods and the proposed method are compared in this section, and the planning results on IEEE 39-bus test system are shown in Table IV, specifically:

Case1: only consider long-term uncertainty.

Case2: only consider seasonal uncertainty.

Case3: consider both long-term and seasonal uncertainty, but seasonal uncertainty is modeled as one single uncertainty set.

Case4: consider both long-term and seasonal uncertainty, and RES seasonal uncertainty are modelled according to seasonal characteristics distribution.

It can be found that the planning cost and annual operation cost of case 3 and case 4 is higher than case 1 and case 2, that is, long-term seasonal uncertainty of RES considered in HES planning framework will result in a larger HES planning result. But considering long-term seasonal uncertainty is necessary, because a high proportion of time-varying RES will result in power balance more influenced by climate conditions. The HES planning results considering long-term seasonal uncertainty of RES are helpful for enhancing the adaptability of power systems to climate variability. Moreover, comparing case 3 and case 4, it can be found that the planning result and operation cost of case 4 is more economical than case 3. In the proposed HES planning framework, the economy of planning results can be further improved by adaptively modelling seasonal uncertainty according to the seasonal characteristics. If RES seasonal uncertainty is not considered according to the seasonal characteristics, power systems need more HES and annual reserve capacity to address RES uncertainty, which will lead to a higher cost.

TABLE IV
PLANNING RESULTS UNDER DIFFERENT CASES

Case	C_{inv} 10^7($)	C_{ope} 10^9($)	P2H/FC (MW)	SHT (t H_2)	Reserve (MW)
1	2.6174	1.5745	197.3	4735.2	0
2	2.1601	1.5769	162.8	3907.2	$2.71*10^6$
3	4.5396	1.7324	342.2	8212.8	$4.55*10^6$
4	3.0218	1.6508	227.8	5466.3	$2.69*10^6$

2) Computational efficiency: to verify the computational efficiency of the proposed hybrid tri-level DRO-ARO model for HES planning in this paper, the computational performance is tested on IEEE 39-bus test system and IEEE 118-bus test system.

TABLE V
THE RESULTS OF COMPUTATIONAL EFFICIENCY

Item	IEEE 39-bus system	IEEE 118-bus system
Number of scenarios N	5	5
CPU time	14419.5 s	21084.98 s
Iteration	3	3

As shown in Table V, the iterations number for both IEEE 39-bus test system and IEEE 118-bus test system are three. The total solution time is 14419.5s on IEEE 39-bus test system and 21084.98s on IEEE 118-bus test system to get the final HES planning results. The computational time does not increase significantly for the larger IEEE 118-bus test system. These results demonstrate the feasibility of the proposed framework on large-scale systems, showing that it can effectively handle complex networks with numerous generation units and RES integration.

Additionally, although the overall CPU time for both IEEE 39-bus test system and IEEE 118-bus test system exceeds four hours to obtain the final HES planning results, the time consumption is acceptable for planning problems. It is worth noting that the longer CPU time is primarily due to the model formulation phase, where the construction of large-scale variables and constraints by Yalmip significantly increases the preprocessing time. While the solving phase using Gurobi remains computationally efficient, highlighting the scalability and practicality of the proposed method.

V. Conclusion

In conclusion, this paper proposes a HES planning framework for addressing the long-term seasonal fluctuations of RES. The problem is formulated as a hybrid tri-level DRO-ARO model. Based on the multi-year RES historical datasets, an ambiguity set of probability distributions is constructed for

representative yearly output scenarios under typical climate conditions, and seasonal uncertainty sets are adaptively modeled to capture seasonal variation patterns. Numerical experiments conducted on the modified IEEE 39-bus and IEEE 118-bus test system demonstrate that considering the long-term seasonal uncertainty of RES leads to a more robust planning strategy. In contrast, adopting a single uncertainty set to characterize RES uncertainty may result in underestimated planning decisions for HES. Moreover, compared with considering seasonal fluctuations using a single unified set, the proposed framework which captures seasonal characteristics achieves a robust planning result at a lower cost. As a key flexible resource in power systems, HES can realize the seasonal regulation and complementation between RES supply and load demand. Additional case studies on IEEE 39-bus and IEEE 118-bus test systems further verify the effectiveness and scalability of the improved C&CG algorithm with duality-free decomposition and adaptive robust reformulation for solving the proposed hybrid tri-level DRO-ARO model for HES planning.

Currently, the proposed model employs representative RES scenarios derived from historical data to characterize RES long-term uncertainty. However, these representative RES scenarios may not adequately capture extreme climate events. To this end, our future research will further focus on extreme climate scenarios in HES planning while AI-based methods will be further explored for more adaptive scenarios generation.

REFERENCES

[1] IEA, "Managing seasonal and inter-annual variability of renewables," [Online]. Available: https://www.iea.org/reports/managing-seasonal-and-interannual-variability-of-renewables.

[2] J. Cronin, G. Anandarajah, O. Dessens, "Climate change impacts on the energy system: a review of trends and gaps," *Climatic Change*, vol. 151, pp. 79–93, 2018.

[3] H. Jiang, E. Du, N. Zhang, Z. Zhuo, P. Wang, Z. Wang, et al, "Renewable Electric Energy System Planning Considering Seasonal Electricity Imbalance Risk," *IEEE Trans. Power Syst.,* vol. 38, no. 6, pp. 5432-5444, Nov. 2023.

[4] D. Zheng, D. Tong, S.J. Davis, et al, "Climate change impacts on the extreme power shortage events of wind-solar supply systems worldwide during 1980–2022," *Nat. Commun.*, vol. 15, pp. 5225-5235, Jun. 2024.

[5] J. Twitchell, K. DeSomber, D. Bhatnagar, "Defining long duration energy storage," *J. Energy Storage*, vol. 60, 2023.

[6] LDES Agency, "Driving to Net Zero Industry Through Long Duration Energy Storage," [Online]. Available: https://www.ldescouncil.com.

[7] A. Z. Arsad, M. A. Hannan, A. Q. Al-Shetwi, et al., "Hydrogen energy storage integrated hybrid renewable energy systems: A review analysis for future research directions," *Int. J. Hydrogen Energy*, vol. 47, no. 39, pp. 17285–17312, 2022.

[8] Hydrogen Council, "Hydrogen scaling up—A sustainable pathway for the global energy transition," [Online]. Available: https://hydrogencouncil.com/wp-content/uploads/2017/11/Hydrogen-Scaling-up_Hydrogen-Council_2017.compressed.pdf.

[9] M. Lu, X. Li, F. Li, W. Xiong, X. Li, "Two-stage stochastic programming of seasonal hydrogen energy storage and mixed hydrogen-fuelled gas turbine system," *Proc. CSEE*, vol. 43, no. 18, pp. 6978–6992, 2023.

[10] Y. Pu, Q. Li, X. Zou, R. Li, L. Li, W. Chen, et al., "Optimal sizing for an integrated energy system considering degradation and seasonal hydrogen storage," *Appl. Energy*, vol. 302, 2021.

[11] Y. Qiu, Q. Li, T. Wang, L. Yin, W. Chen, H. Liu, "Optimal planning of cross-regional hydrogen energy storage systems considering the uncertainty," *Appl. Energy*, vol. 326, 2022.

[12] G. Pan, W. Gu, Y. Lu, H. Qiu, S. Lu, S. Yao, "Optimal planning for electricity-hydrogen integrated energy system considering power to hydrogen and heat and seasonal storage," *IEEE Trans. Sustain. Energy*, vol. 11, pp. 2662–2676, 2020.

[13] Z. Shao, X. Cao, Q. Zhai, X. Guan, "Risk-constrained planning of rural-area hydrogen-based microgrid considering multiscale and multi-energy storage systems," *Appl. Energy*, vol. 334, 2023.

[14] H. Jiang, B. Qi, E. Du, N. Zhang, X. Yang, F. Yang, et al., "Modelling hydrogen supply chain in renewable electric energy system planning," *IEEE Trans. Ind. Appl.*, vol. 58, pp. 2780–2791, 2022.

[15] X. Wu, B. Cao, B. Liu, X. Wang, "A planning model of standalone hydrogen-based carbon-free microgrid through convex relaxation," *IEEE Trans. Smart Grid*, vol. 14, pp. 2668–2680, 2023.

[16] J. Li, J. Lin, H. Zhang, Y. Song, G. Chen, L. Ding, et al., "Optimal investment of electrolyzers and seasonal storages in hydrogen supply chains incorporated with renewable electric networks," *IEEE Trans. Sustain. Energy*, vol. 11, pp. 1773–1784, 2020.

[17] S. Jiang, S. Wen, M. Zhu, Y. Huang, H. Ye, "Scenario-transformation-based optimal sizing of hybrid hydrogen-battery storage for multi-timescale islanded microgrids," *IEEE Trans. Sustain. Energy*, vol. 14, pp. 1784–1795, 2023.

[18] N. Zhang, H. Jiang, E. Du, Z. Zhuo, P. Wang, Z. Wang, et al., "An efficient power system planning model considering year-round hourly operation simulation," *IEEE Trans. Power Syst.*, vol. 37, pp. 4925–4935, 2022.

[19] J. Zhao, Q. Zhai, Y. Zhou, L. Wu and X. Guan, "Adaptive Characteristic Modeling of Long-Period Uncertainties: A Multi-Stage Robust Energy Storage Planning Approach Based on the Finite Covering Theorem," *IEEE Trans. Sustain. Energy*, vol. 15, no. 4, pp. 2393-2404, Oct. 2024.

[20] M. A. Russo, D. Carvalho, N. Martins, A. Monteiro, "Future perspectives for wind and solar electricity production under high-resolution climate change scenarios," *J. Clean. Prod.*, vol. 404, pp. 136997, 2023,

[21] L. Liu, G. He, M. Wu, et al., "Climate change impacts on planned supply–demand match in global wind and solar energy systems," *Nat. Energy*, vol. 8, pp. 870–880, 2023.

[22] A.T.D. Perera, V.M. Nik, D. Chen, et al. Quantifying the impacts of climate change and extreme climate events on energy systems. *Nat. Energy,* vol 5, pp. 150–159, 2020.

[23] J. Yan, B. Hu, K. Xie, J. Tang and H. Tai, "Data-Driven Transmission Defense Planning Against Extreme Weather Events*," IEEE Trans. on Smart Grid*, vol. 11, no. 3, pp. 2257-2270, May 2020.

[24] Q. Sun, Z. Wu, W. Gu, X.-P. Zhang, P. Liu, G. Pan, et al., "Tri-level multi-energy system planning method for zero energy buildings considering long and short-term uncertainties," *IEEE Trans. Sustain. Energy*, vol. 14, pp. 339–355, 2023.

[25] Y. Zhou, J. Zhao, Y. Song, J. Sun, H. Fu, M. Chu, "A seasonal-trend-decomposition-based voltage-source-inverter open-circuit fault diagnosis method," *IEEE Trans. Power Electron.*, vol. 37, pp. 15517–15527, 2022.

[26] Q. Hu, G. Li, S. Sun, Z. Bie, "Incorporating catastrophe insurance in power distribution systems investment and planning for resilience enhancement," *Int. J. Electr. Power Energy Syst.*, vol. 155, pp. 109438, 2024.

[27] C. Zhao, Y. Guan, "Data-driven stochastic unit commitment for integrating wind generation," *IEEE Trans. Power Syst.*, vol. 31, pp. 2587–2596, 2016.

[28] J. Wang, L. Chen, Z. Tan, et al., "Inherent spatiotemporal uncertainty of renewable power in China," *Nat. Commun.*, vol. 14, p. 5379, 2023.

[29] M. Qu, T. Ding, C. Mu, Y. Sun, P. Siano, M. Shahidehpour, "Adjustable robust low-carbon unit commitment with nonanticipativity by linear programming," *IEEE Trans. Netw. Sci. Eng.*, early access, pp. 1–14, Jun. 2023, doi: 10.1109/TNSE.2023.3281072.

[30] L. Jiang, Z. Bie, T. Long, X. Wang, H. Xie, G. Li, "A post-event generator start-up strategy for renewable penetrated transmission system considering dynamic frequency regulation," *IEEE Trans. Sustain. Energy*, vol. 14, no. 2, pp. 1135–1150, Apr. 2023.

[31] B. Zeng, L. Zhao, "Solving two-stage robust optimization problems using a column-and-constraint generation method," *Oper. Res. Lett.*, vol. 41, pp. 457–461, 2013.

[32] R. A. Jabr, "Adjustable robust OPF with renewable energy sources," *IEEE Trans. Power Syst.*, vol. 28, no. 4, pp. 4742–4751, Nov. 2013.

[33] T. Ding, Q. Yang, X. Liu, C. Huang, Y. Yang, M. Wang, et al., "Duality-free decomposition-based data-driven stochastic security-constrained unit commitment," *IEEE Trans. Sustain. Energy*, vol. 10, pp. 82–93, 2019.

[34] Illinois, "IEEE 39-Bus System" [EB/OL], [2024-08-11]. Available: https://icseg.iti.illinois.edu/ieee-39-bus-system.

[35] Illinois, "IEEE 118-Bus System" [EB/OL], [2025-03-11]. Available: https://icseg.iti.illinois.edu/ieee-118-bus-system.